Mechanisms of Altered Excitation-Contraction Coupling in Canine Tachycardia-Induced Heart Failure, II
Model Studies

Raimond L. Winslow, Jeremy Rice, Saleet Jafri, Eduardo Marbán, Brian O'Rourke

Abstract—Ca^{2+} transients measured in failing human ventricular myocytes exhibit reduced amplitude, slowed relaxation, and blunted frequency dependence. In the companion article (O'Rourke B, Kass DA, Tomaselli GF, Kääb S, Tunin R, Marbán E. Mechanisms of altered excitation-contraction coupling in canine tachycardia-induced heart, I: experimental studies. *Circ Res*. 1999;84:562–570), O'Rourke et al show that Ca^{2+} transients recorded in myocytes isolated from canine hearts subjected to the tachycardia pacing protocol exhibit similar responses. Analyses of protein levels in these failing hearts reveal that both SR Ca^{2+} ATPase and phospholamban are decreased on average by 28% and that Na^+/Ca^{2+} exchanger (NCX) protein is increased on average by 104%. In this article, we present a model of the canine midmyocardial ventricular action potential and Ca^{2+} transient. The model is used to estimate the degree of functional upregulation and downregulation of NCX and SR Ca^{2+} ATPase in heart failure using data obtained from 2 different experimental protocols. Model estimates of average SR Ca^{2+} ATPase functional downregulation obtained using these experimental protocols are 49% and 62%. Model estimates of average NCX functional upregulation range are 38% and 75%. Simulation of voltage-clamp Ca^{2+} transients indicates that such changes are sufficient to account for the reduced amplitude, altered shape, and slowed relaxation of Ca^{2+} transients in the failing canine heart. Model analyses also suggest that altered expression of Ca^{2+} handling proteins plays a significant role in prolongation of action potential duration in failing canine myocytes. (*Circ Res*. 1999;84:571-586.)

Key Words: excitation-contraction coupling ■ heart failure ■ midmyocardial ventricular action potential ■ Ca^{2+} transient

Recent studies using the canine tachycardia pacing-induced model of heart failure[1–8] demonstrate that changes in cellular electrophysiological and excitation-contraction (E-C) coupling processes are qualitatively similar to those observed in cells isolated from failing human heart. In human heart failure, I_{K1} current density measured at hyperpolarized membrane potentials is reduced by $\approx$50%,[9,10] and density of the transient outward current I_{to1} is reduced by $\approx$75% in subepicardial[11] and $\approx$40% in midmyocardial ventricular cells[9] and is unchanged in subendocardial ventricular cells.[11] The magnitude of I_{K1} is reduced by $\approx$40%, and that of I_{to1} by $\approx$70% in failing canine midmyocardial cells.[5] Expression of proteins involved in E-C coupling is also altered in human heart failure. Sarcoplasmic reticulum (SR) Ca^{2+} AT-Pase mRNA level,[12–16] protein level,[12,17,18] and uptake rate[19] are reduced by $\approx$50% in end-stage heart failure. Na^+/Ca^{2+} exchanger (NCX) mRNA levels are increased by $\approx$55% to 79%,[12,20] and NCX protein levels increase 36% to 160%.[12,20–22]

Less information is available with regard to NCX function in heart failure. However, Reinecke et al[22] reported an 89% increase in sodium-gradient–stimulated $^{45}Ca^{2+}$ uptake in human heart sarcolemmal vesicles.

As described in the preceding article by O'Rourke et al,[23] alterations of intracellular Ca^{2+} handling in failing canine midmyocardial ventricular myocytes parallel those observed in human. In particular, the time constant of Ca^{2+} uptake in the absence of Na^+/Ca^{2+} exchange is prolonged in failing cells (576 ± 83 versus 282 ± 30 ms in controls), suggesting a functional downregulation of the SERCA2a. This observation is consistent with Western blot analyses indicating that SR Ca^{2+} ATPase protein levels are reduced in failing heart by 28%. Additionally, in the presence of cyclopiazonic acid (CPA, a blocker of the SR Ca^{2+} ATPase pump), the time constant of Ca^{2+} extrusion is larger in normal than failing cells (813 ± 269 versus 599 ± 48 ms). This observation is consistent with Western blot analyses indicating a 104%

Circulation Research is available at http://www.circresaha.org

increase in the level of expression of the NCX in failing cells. Taken together, these results suggest that SR Ca²⁺ uptake is impaired and that Ca²⁺ extrusion via the NCX is enhanced in myocytes isolated from the failing canine heart in a way that is similar qualitatively to that seen in human patients.

In this article, we use the data of O'Rourke et al[23] to develop a computational model of the action potential and of intracellular Ca²⁺ handling in normal and failing canine ventricular myocytes using biophysically detailed descriptions of both sarcolemmal currents and key components of E-C coupling. With the limits of individual alterations fixed using experimentally derived values, the model is used to quantify the extent to which each parameter (I_{to1}, I_{K1}, SR Ca²⁺ ATPase, and NCX) contributes to the overall change in electrical and Ca²⁺ dynamics in heart failure. The results support the hypothesis that differences in expression of sarcolemmal ion channels and Ca²⁺ handling proteins measured experimentally are sufficient to account for the altered action potential waveform and Ca²⁺ transient of the failing canine cardiomyocyte.

Materials and Methods

Normal Canine Ventricular Cell Model

Jafri et al[24] have presented a model of Ca²⁺ handling in the guinea pig ventricular myocyte that incorporates the following: (1) sarcolemmal ion currents of the Luo-Rudy phase II ventricular cell model,[25] (2) a state model of the L-type Ca²⁺ current in which Ca²⁺-mediated inactivation occurs via the mechanism of mode switching,[26] (3) calcium-induced calcium release from SR via ryanodine-sensitive calcium release (RyR) channels using a model adapted from that of Keizer and Levine,[27] and (4) a restricted subspace located between the junctional SR (JSR) and T tubules into which both L-type Ca²⁺ and RyR channels empty. The model of the canine midmyocardial ventricular cell used in this study is derived from this guinea pig ventricular cell model. All dynamic equations, parameters, and initial conditions for this new model are given in the Appendix. The following modifications to the model of Jafri et al[24] have been made to better represent properties of canine midmyocardial ventricular cells.

I_{to1}

Canine epicardial and midmyocardial ventricular cell action potentials exhibit a prominent notch in phase 1 of the action potential that results from the presence of 2 transient outward currents: a Ca²⁺-independent 4-aminopyridine (4-AP)–sensitive current (I_{to1})[5,28,29] and a Ca²⁺-dependent current (I_{to2}).[29,30] The Ca²⁺-independent component I_{to1} is modeled on the basis of the formulation of Campbell et al[31] for ferret ventricular cells. Peak I_{to1} conductance (G_{to1}) was adjusted to yield a linear plot of peak current density in response to 500-ms–duration voltage-clamp stimuli from a holding potential of −80 mV, with slope 0.3 pA/pF-mV and y-intercept 4.6 pA/pF. This agrees well with experimental measurements reported for canine I_{to1} at 37°C by Liu et al[28] (see their Figure 10B: slope, 0.28 pA/pF-mV, and y-intercept, 5 pA/pF). Activation rate constants were scaled to yield a time to peak of ≈8 ms at a clamp potential of +10 mV (see Figure 5B of Tseng and Hoffman).[29] Inactivation rate constants were adjusted to yield a decay time constant of ≈20 ms.[29] The Ca²⁺-dependent chloride (Cl–) current I_{to2} was not incorporated in this model.

I_{Kr}

The delayed rectifier current I_K in both canine and guinea pig ventricular myocytes consists of rapid- and slow-activating components known as I_{Kr} and I_{Ks}, respectively. Models of I_{Kr} and I_{Ks} in guinea pig ventricular cells have been developed.[32] These models have been modified to approximate properties of corresponding currents measured in isolated canine midmyocardial ventricular cells. I_{Kr} is described using a closed-open–state model in which forward (K_{12}) and backward (K_{21}) rate constants are exponential functions of voltage (V) with the following form:

$$(1) \qquad K_{ij}(V) = e^{a_{ij} + b_{ij}V}.$$

Parameters of this model are fully constrained by knowledge of the time constant $\tau(V)$, defined as

$$(2) \qquad \tau(V) = \frac{1}{K_{12}(V) + K_{21}(V)},$$

at 2 voltages and by knowledge of the steady-state activation function. Activation was fit using a Boltzmann function determined by Liu and Antzelevitch[33] (see their Figure 11). The time constant of activation at +5 mV was set to 100 ms,[33] and the time constant of deactivation at −60 mV was set to 3000 ms,[34] thereby constraining the rate constants $K_{12}(V)$ and $K_{21}(V)$. A fixed increment of 27 ms was added to Equation 2 to bound the time constant away from 0 at depolarized potentials. The maximum conductance $\overline{G}_{Kr}$ was adjusted to yield a tail current density of 0.2 pA/pF in response to a voltage-clamp step to +25 mV for 3.0 seconds, followed by a step to −35 mV for 1.0 seconds, as described by Gintant.[35]

I_{Ks}

The slow-activating delayed rectifier current I_{Ks} is present in epicardial, midmyocardial, and endocardial canine ventricular cells. I_{Ks} is modeled as described in Zeng et al,[32] with the exception that the steady-state activation function is fit using a Boltzmann function determined by Liu and Antzelevitch.[33] The voltage-dependent time constant is also shifted by +40 mV in the depolarizing direction to fit the experimental data of Liu and Antzelevitch[33] (see their Figure 13). Maximum conductance ($\overline{G}_{Ks}$) is adjusted to yield a tail current density of 0.4 pA/pF in response to 3.0-second–duration voltage-clamp steps from the holding potential of −35 to +25 mV, followed by a return to the holding potential[34] (see Figure 5). The Ca²⁺ dependence of I_{Ks} described in the Luo-Rudy phase II guinea pig model is not included, as there are no experimental data constraining this dependence in canine ventricular cells.

I_{K1}

I_{K1} is fit using data measured at 22°C in isolated canine midmyocardial ventricular myocytes measured by Kääb et al[5] and scaled to 37°C. These data indicate that maximum outward I_{K1} density is ≈2.5 pA/pF at −60 mV[5] (see Reference 5, Figure 4B). These data also show that I_{K1} density is nonnegligible at voltages within the plateau range of the canine action potential. For example, I_{K1} density is 0.3 pA/pF at 0 mV, a value comparable with the density of I_{Kr} during the plateau phase of the action potential. The functional representation of I_{K1} in the Luo-Rudy phase II model can therefore not be used, as it approaches 0 at plateau membrane potentials. An alternative formulation better approximating the canine data is presented in the Appendix.

$I_{Ca,L}$

The model of L-type Ca²⁺ current used is identical to the mode-switching model presented in Jafri et al,[24] with 3 exceptions. First, the voltage dependence of the activation transition rates $\alpha(V)$ and $\beta(V)$ and the inactivation variable $y(V)$ are shifted by +10 mV in the depolarizing direction to position the peak L-type Ca²⁺ current in response to voltage-clamp stimuli at +5 mV, as measured experimentally.[5] Second, the monotonic decreasing steady-state (voltage-dependent) inactivation function y_∞ is modified to have an asymptotic value of 0.2 for large positive membrane potentials V. This modification reproduces the slow component of Ca²⁺ current observed under voltage-clamp stimuli in canine ventricular cells.[5,37] Finally, peak L-type Ca²⁺ current density is adjusted to a value of 2.5 pA/pF at a clamp voltage of +5 mV.

J_{up}

In the model of Jafri et al,[24] Ca²⁺ uptake into network SR (NSR) is modeled using a Hill function with coefficient of 2. Reverse pump

rate is assumed to be 0, and Ca^{2+} leak from NSR to cytoplasm is assumed to be proportional to the gradient of NSR and cytosolic Ca^{2+} concentrations. Recently, Shannon et al[38] have proposed the hypothesis that SR Ca^{2+} accumulation at rest is not limited by leak of Ca^{2+} from SR but rather is limited by a reverse component of SR Ca^{2+} ATPase pump current. They have proposed a new model of the SR Ca^{2+} ATPase pump that includes forward- and reverse-current components, each with its own binding constant and peak forward and reverse rates (denoted V_{maxf} and V_{maxr}, respectively).[39] The forward mode exhibits slight cooperativity, whereas the reverse mode is noncooperative. The relative magnitudes of forward- and reverse-current components determine whether SR load increases, is constant, or decreases during diastole. The model is presented in the Appendix.

Failing Canine Ventricular Cell Model

Kääb et al[5] have shown that in the canine tachycardia pacing-induced model of heart failure, I_{to1} and I_{K1} are downregulated on average by 66% and 32%, respectively, in terminal heart failure. Only the number of expressed channels is changed; the kinetic properties of I_{to1} and gating behavior of I_{K1} are unaltered. On the basis of these data, the effects of terminal heart failure are modeled by reducing the peak conductance of I_{to1} and I_{K1} by the factors indicated above. Downregulation of the SR Ca^{2+} ATPase is modeled by simultaneous scaling of both the forward and reverse maximum pump rates V_{maxf} and V_{maxr} by a scale factor, K_{SR}. Upregulation of the NCX is modeled by increasing a scale factor, K_{NaCa}.

Numerical Methods

The dynamical equations in the Appendix are solved on a Silicon Graphics workstation using the Merson modified Runge-Kutta fourth-order adaptive step algorithm (No. 25, Reference 52), with a maximum step size of 100 microseconds and maximum error tolerance of 10^{-6}. The error from all variables is normalized to ensure that each contributes equally to the calculation of global error, as described in Jafri et al.[24] Initial conditions listed in the Appendix are used in all calculations, unless noted otherwise. These initial conditions were computed in response to a periodic pulse train of frequency 1 Hz and were determined immediately before the 11th pulse. Action potentials are initiated using 0.1 $\mu A\mu F^{-1}$ current injection for 500 microseconds.

The canine ventricular cell model is used to derive quantitative estimates of the NCX scale factor K_{NaCa} and the SR Ca^{2+} ATPase scale factor K_{SR} from experimental data by fitting model Ca^{2+} transient decay rates to those measured experimentally. To do this, a series of 10 voltage-clamp stimuli (–97-mV holding potential, 3-mV step potential, and 200-ms duration) are applied at a frequency of 1 Hz. Ca^{2+} transient decay rate is estimated from response to the final voltage-clamp stimulus to assure that model SR Ca^{2+} concentrations have reached equilibrium values.

Results

Action Potentials and Ca²⁺ Transients: Model Versus Experimental Results

Figure 1 demonstrates the ability of the model to reconstruct action potentials and Ca^{2+} transients of both normal and failing canine midmyocardial ventricular myocytes. The solid and dotted lines in Figure 1A show experimental measurements of normal and failing action potentials, respectively. Model action potentials are shown in Figure 1C. In this figure, the solid line shows a normal action potential. The dashed line shows an action potential when I_{to1} is reduced by 66% of the normal values and I_{K1} by 32% of the normal values (the average percentage reductions observed in terminal heart failure.)[5] The dotted line corresponds to these same reductions of I_{to1} and I_{K1}, in addition to a 62% reduction of the SR Ca^{2+} ATPase pump and a

75% increase of the NCX. These values are model-based estimates of the average percentage change in activity of these proteins determined using experimentally derived limits on their function, as described in the following sections.

The model data of Figure 1C show that downregulation of I_{to1} and I_{K1} reduces the depth of the phase 1 notch. However, notch depth is larger in the experimental measurements from the failing myocyte (Figure 1A, dotted line) than is predicted by the model (Figure 1C, dashed line). This greater notch depth is due to the presence of the Ca^{2+}-dependent transient outward current I_{to2}, which is not included in the model. The most significant change in model action potential duration (APD) occurs with upregulation of the NCX and downregulation of the SR Ca^{2+} ATPase (Figure 1C, dotted line). These 2 changes alone increase APDs at 90% repolarization (APD_{90}) by ≈200 ms.

Figure 1D illustrates model normal (solid line) and failing (dotted line) Ca^{2+} transients. Amplitude of the Ca^{2+} transient is reduced significantly in the heart failure model. Ca^{2+} transient shape is flattened, duration is prolonged, and relaxation is slowed. These changes are similar qualitatively to those seen in the experimental data of Figure 1B.

Figures 1E and 1F show L-type Ca^{2+} and Na^+/Ca^{2+} exchange currents for normal (solid lines) and failing (dotted lines) model cells. The reduction in peak magnitude of the L-type Ca^{2+} current seen in Figure 1E for the failing model cell results from downregulation of I_{to1}, which reduces depth of the phase 1 notch and therefore driving force during onset of the L-type Ca^{2+} current. Figure 1E also shows that L-type Ca^{2+} current is increased during the later plateau phase of the action potential in failing model cells. The mechanism of this increase will be considered in subsequent sections. Figure 1F shows that Na^+/Ca^{2+} exchange operates in reverse mode, generating a net outward current during most of the plateau phase of the action potential. The magnitude of this outward current decreases during the plateau phase, and in the failing cell model the current becomes significantly smaller than the inward L-type Ca^{2+} current.

These simulations demonstrate the ability of the model to reproduce both normal and failing canine myocyte action potentials and Ca^{2+} transients. The following sections describe application of the model to estimation of the degree of functional change in the NCX and SR Ca^{2+} ATPase in control and failing myocytes. The approach is as follows: (1) the time constant of Ca^{2+} decay (τ_{Ca}) measured with SR function blocked using CPA data is used to estimate the model Na^+/Ca^{2+} exchange scale factor K_{NaCa}; (2) with K_{NaCa} fixed at this value, the model SR Ca^{2+} ATPase scale factor K_{SR} required to reproduce the τ_{Ca} measured in physiological solutions is determined; (3) the SR Ca^{2+} ATPase reduction in heart failure is cross-checked independently by determining the model SR Ca^{2+} ATPase scale factor required to reproduce the τ_{Ca} measured under Na^+-free conditions (0-Na data) with the model Na^+/Ca^{2+} exchange set to 0; and (4) the model Na^+/Ca^{2+} exchange scale factor is estimated independently from τ_{Ca} in physiological solutions using the estimate of SR function determined in step 3.
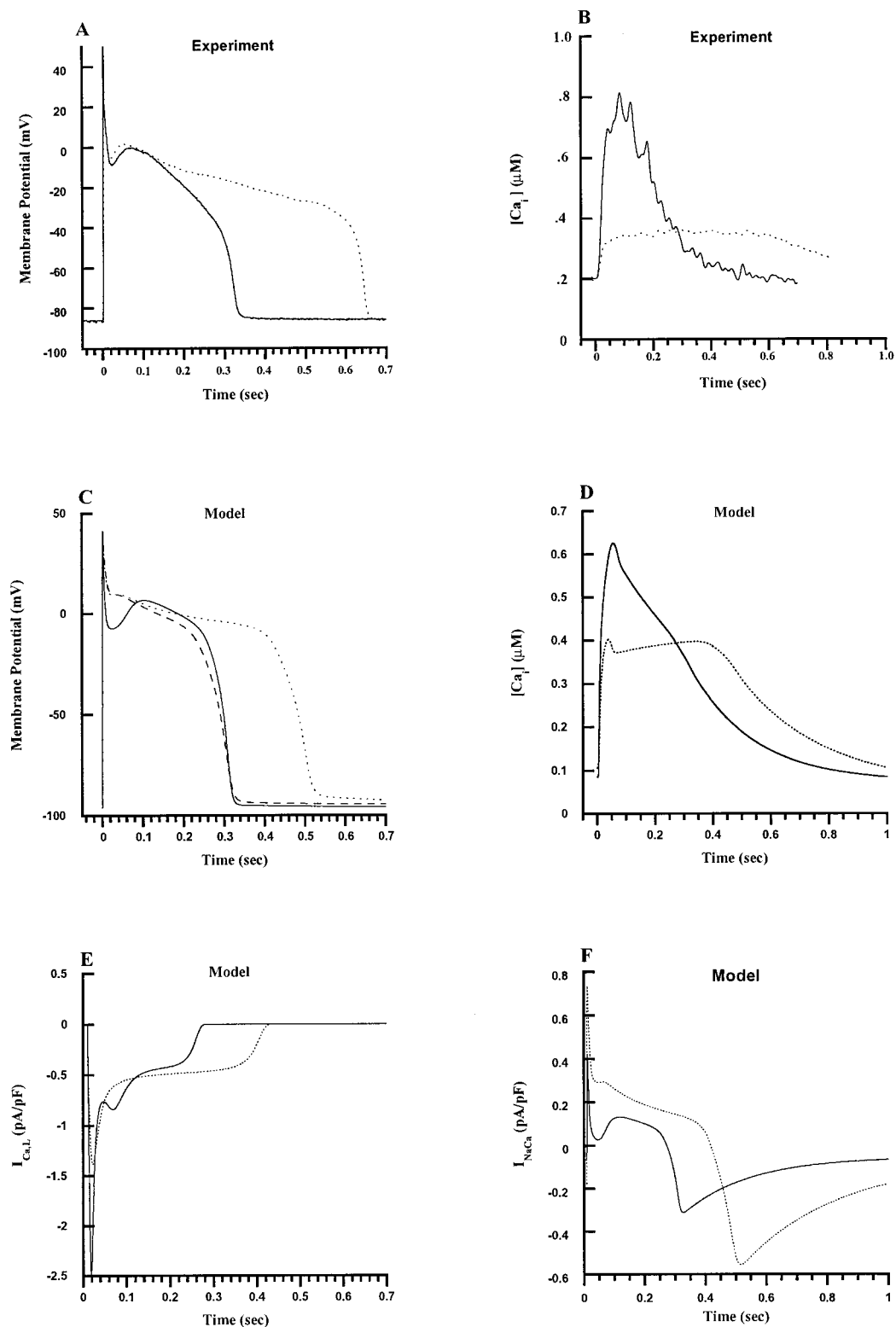
Figure 1. Model vs experimental action potentials and Ca^{2+} transients. Each action potential and Ca^{2+} transient is in response to a 1-Hz pulse train, with responses measured in the steady state. A, Experimentally measured membrane potential as a function of time in normal (solid line) and failing (dotted line) canine myocytes. B, Experimentally measured cytosolic Ca^{2+} concentration (μmol/L) as a function of time for normal (solid line) and failing (dotted line) canine ventricular myocytes. C, Membrane potential as a function of time simulated using the normal canine myocyte model (solid line), the myocyte model with I_{to1} and I_{K1} downregulation (dashed line; downregulation by 66% and 32%, respectively), and the heart failure model (dotted line; downregulation of I_{to1} and I_{K1} as described previously, K_{SR}=0.38 corresponding to 62% downregulation and K_{NaCa}=0.53 corresponding to 75% upregulation). D, Cytosolic Ca^{2+} concentration (μmol/L) as a function of time simulated using the normal (solid line) and heart failure (dotted line) model, with parameters as described in panel A. E, L-type Ca^{2+} current as a function of time for the normal (solid line) and failing (dotted line) cell models. F, Na^{+}/Ca^{2+} exchange current as a function of time for the normal (solid line) and failing (dotted line) cell models.
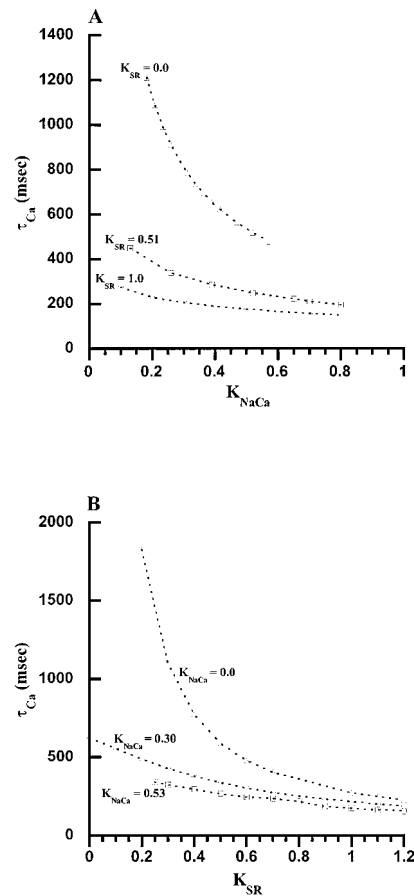
Figure 2. A, Model voltage-clamp Ca^{2+} transient relaxation time constant τ_{Ca} as a function of NCX scale factor K_{NaCa} at SR Ca^{2+} ATPase pump scale factors of K_{SR}=0.0 (corresponding to CPA block), 0.51 (value estimated in 0-Na experiments for failing myocytes), and 1.0 (normal value). △ indicates K_{SR}=0.0; □, K_{SR}=0.51; and ○, K_{SR}=1.0. B, Model Ca^{2+} transient relaxation time constant τ_{Ca} as a function of SR Ca^{2+} ATPase pump scale factor K_{SR} for K_{NaCa} values of 0.0 (0-Na conditions), 0.30 (value estimated in normal myocytes in presence of CPA), and 0.53 (value estimated for failing myocytes during CPA block). △ indicates K_{NaCa}=0.0; □, K_{NaCa}=0.53; and ○, K_{NaCa}=0.30.

Estimation of NCX and SR Ca^{2+} ATPase Activity in Normal and Failing Myocytes: CPA Experiments

In the preceding article by O'Rourke et al, Ca^{2+} transients in response to voltage-clamp stimuli were measured in the presence and absence of CPA, a blocker of the SR Ca^{2+} ATPase pump. In the presence of CPA, Ca^{2+} transient decay rate (τ_{Ca}) following termination of a depolarizing voltage step reflects the rate of extrusion of Ca^{2+} from the cytosol by the NCX (extrusion by the sarcolemmal Ca^{2+} ATPase is small). Estimates of the NCX pump current scale factor K_{NaCa} may therefore be obtained by setting the model value of K_{SR} to 0 and varying K_{NaCa} until model Ca^{2+} transient decay rates match those measured experimentally in the presence of CPA. K_{NaCa} may then be fixed at this value and K_{SR} varied until model Ca^{2+} transient decay rate matches that measured experimentally using physiological solutions. This procedure can be applied to data obtained from both normal and failing cells to assess the extent of functional upregulation and

downregulation of the NCX and SR Ca^{2+} ATPase in heart failure.

To estimate K_{NaCa}, model K_{SR} was set to 0, 10 voltage-clamp steps (holding potential −97 mV, step potential 3 mV, and duration 200 ms) were applied at a frequency of 1 Hz to assure that Ca^{2+} levels in each model Ca^{2+} pool were equilibrated, and model τ_{Ca} was measured by fitting an exponential function to the decay phase of the final Ca^{2+} transient. Figure 2A plots model τ_{Ca} (ordinate, ms) as a function of K_{NaCa} (abscissa) with K_{SR}=0.0 (open triangles). K_{NaCa}=0.30 yields a τ_{Ca} equal to the average value measured experimentally in normal myocytes in the presence of CPA (813±269 ms). One SD of experimental variability is accounted for by K_{NaCa} values in the interval (0.21, 0.48). This same curve shows that K_{NaCa}=0.53 produces a τ_{Ca} matching that measured in failing myocytes in the presence of CPA (599±48 ms). One SD experimental variability is encompassed by K_{NaCa} values in the interval (0.48, 0.60). Assuming the normal value of K_{NaCa} to be 0.30, these data suggest a functional upregulation of the NCX in heart failure in the range of 60% to 100%, with average value ≈75%.

Figure 2B plots model τ_{Ca} (ordinate, ms) as a function of K_{SR} (abscissa). The curve marked with open circles plots this dependence when K_{NaCa} is constant at the normal value estimated above (K_{NaCa}=0.30). The experimental value of τ_{Ca} measured in normal myocytes using physiological solutions is 219±36 ms. The maximum forward and reverse SR Ca^{2+} ATPase pump rates V_{maxf} and V_{maxr} given in Table 4 of the Appendix have been selected to yield a similar time constant when K_{SR}=1.0. Measured variation about this value is accounted for by K_{SR} values in the interval (0.85, 1.15).

The experimental value of τ_{Ca} measured in failing myocytes using physiological solutions is 292±23 ms. Dependence of model τ_{Ca} on K_{SR} when K_{NaCa} is fixed at the value estimated for failing canine myocytes (0.53) is shown by the curve labeled with open squares in Figure 2B. K_{SR}=0.38 yields a model τ_{Ca} equal to that observed experimentally. The experimental deviation of τ_{Ca} is accounted for by K_{SR} values in the interval (0.26, 0.51). Assuming the average value of K_{SR} in normal cells to be 1.0, these data suggest a functional downregulation of the SR Ca^{2+} ATPase pump in heart failure in the range of 49% to 74%, with average value 62%.

Estimation of NCX and SR Ca^{2+} ATPase Activity in Normal and Failing Myocytes: 0-Na Experiments

To provide a second, independent measure of altered Ca^{2+} handling protein expression in heart failure, O'Rourke et al[23] have measured τ_{Ca} in the presence and absence of Na$^+$/Ca^{2+} exchange by removing Na$^+$ ions from both intracellular and extracellular solutions. In the absence of Na$^+$/Ca^{2+} exchange, τ_{Ca} reflects primarily the rate of Ca^{2+} uptake from the cytosol by the SR Ca^{2+} ATPase pump. Estimates of the SR Ca^{2+} ATPase pump rate scale factor K_{SR} under 0-Na conditions may therefore be obtained by setting the model value of K_{NaCa} to 0 and varying K_{SR} until simulated voltage-clamp Ca^{2+} transient decay rates match those measured experimentally. Once the model value of K_{SR} is constrained, K_{NaCa} can then be determined by changing its value until model Ca^{2+} transient

decay rates match those measured experimentally using physiological solutions. This procedure can be applied to data obtained from both normal and failing cells to assess the extent of functional upregulation and downregulation of the NCX and SR Ca^{2+} ATPase in heart failure.

To mimic 0-Na conditions, K_{NaCa} was set equal to 0. K_{SR} was then varied, and the time constant for Ca^{2+} reuptake into SR was computed. Model τ_{Ca} values are plotted as a function of K_{SR} in Figure 2B (open triangles). Experimentally measured values of this time constant are 282 ± 30 ms in normal and 576 ± 83 ms in failing canine ventricular cells studied under 0-Na conditions. A K_{SR} value of 1.0 accounts for τ_{Ca} measured experimentally in normal cells (282 ± 30 ms), and values in the interval (0.92, 1.07) account for the observed SD in these measurements. This estimate of the average K_{SR} value in normal myocytes based on block of the NCX agrees with that estimated using the CPA data. A K_{SR} value of 0.51 accounts for the average τ_{Ca} measured experimentally in failing cells (576 ± 83 ms), and K_{SR} values in the interval (0.46, 0.59) account for the SD. Assuming the normal K_{SR} value to be 1.0, these data suggest a functional downregulation of the SR Ca^{2+} ATPase pump in failing myocytes in the range of 41% to 54%, with average value 49%. This estimate of SR Ca^{2+} ATPase downregulation is qualitatively similar to that obtained using CPA.

Dependence of model τ_{Ca} on K_{NaCa} when K_{SR} is fixed at the value estimated for normal canine myocytes (1.0) is shown by the curve labeled with open circles in Figure 2A. $K_{NaCa}=0.22$ yields a model τ_{Ca} equal to that observed experimentally using physiological solutions (219 ± 36 ms). Experimental deviation of τ_{Ca} is accounted for by K_{NaCa} values in the interval (0.13, 0.43). Dependence of model τ_{Ca} on K_{NaCa} when K_{SR} is fixed at the value estimated for failing canine myocytes under 0-Na conditions (0.51) is shown by the curve labeled with open squares in Figure 2A. $K_{NaCa}=0.35$ yields a model τ_{Ca} equal to the average value observed experimentally using physiological solutions (292 ± 23 ms). Experimental deviation of τ_{Ca} is accounted for by K_{NaCa} values in the interval (0.26, 0.46). Assuming the normal value of K_{NaCa} to be 0.22, these data suggest a functional upregulation of the NCX in heart failure in the range of 18% to 109%, with average value 38%. This estimate of altered expression of NCX in heart failure has greater variability than that obtained previously using the CPA data but is consistent in that it also indicates increased expression.

Parametric Dependence of Voltage-Clamp Ca^{2+} Transients on SR Ca^{2+} ATPase and NCX Levels

The above analyses provide estimates of K_{SR} and K_{NaCa} in normal and failing myocytes. Results indicate functional downregulation of the SR Ca^{2+} ATPase pump and upregulation of the NCX in heart failure. The parametric dependence of model cytosolic Ca^{2+} transients on K_{SR} and K_{NaCa} is examined next.

Model cytosolic Ca^{2+} concentration (ordinate, μmol/L) versus time (abscissa, seconds) is shown in Figure 3A as K_{SR} is varied. In these simulations, K_{NaCa} is constant at the value estimated using CPA data from normal cells ($K_{NaCa}=0.30$). K_{SR} is varied from 1.0 to 0.0 in steps of 0.1. Ca^{2+} transients
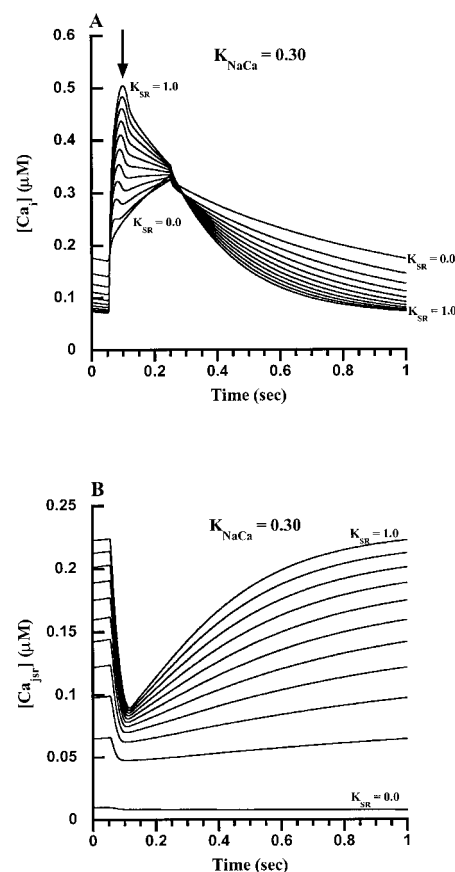

Figure 3. A, Cytosolic Ca^{2+} concentration (μmol/L) as a function of time in response to a 10-second–duration periodic sequence of voltage-clamp stimuli with frequency of 1 Hz. Holding potential is –97 mV, and clamp potential is +3 mV, with duration of 200 ms. Only response to the final stimulus is shown. A family of responses is shown in which K_{NaCa} is constant at 0.30 (value estimated in CPA experiments with normal canine myocytes), and K_{SR} is varied from 1.0 to 0.0 in steps of 0.1. B, Model JSR Ca^{2+} concentration in response to the stimuli in panel A.

are in response to a 1-Hz voltage-clamp stimulus (holding potential –97 mV, step potential 3 mV, and duration 200 ms). Response to the final stimulus of 10 stimulus cycles is shown, with the time origin translated to 0 seconds. These data show that reduction of the model SR Ca^{2+} ATPase pump, simulating the effects of downregulation of this pump in heart failure, reduces the amplitude of the early peak of the Ca^{2+} transient (marked by the arrow). This early peak disappears as K_{SR} approaches 0. Figure 3B shows JSR Ca^{2+} levels for each of the responses in Figure 3A. Reduction of the early peak in the data of Figure 3A coincides with depletion of JSR Ca^{2+} at small values of K_{SR}. Thus, the early peak in the model Ca^{2+} transient is generated by Ca^{2+} release from JSR, and the slow second peak, which is present even when JSR is depleted, results from influx of Ca^{2+} through sarcolemmal L-type Ca^{2+} channels and reverse-mode Na^+/Ca^{2+} exchange. As K_{SR} decreases, Ca^{2+} levels in JSR decrease, and the Ca^{2+} transient becomes reduced in peak amplitude. The Ca^{2+} transient exhibits a decrease, no change, or an increase of amplitude during the course of the voltage-clamp stimulus, depending on the value of K_{SR}. Decay rate of the Ca^{2+} transient decreases
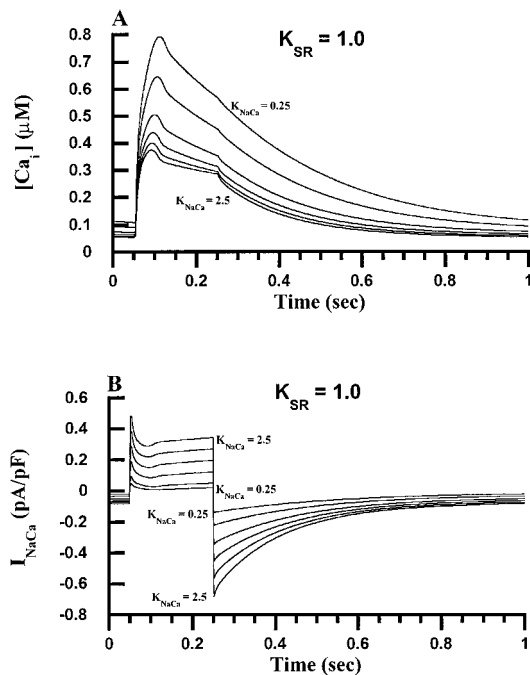
Figure 4. A, Cytosolic Ca^{2+} concentration (μmol/L) as a function of time in response to a 10-second–duration periodic sequence of voltage-clamp stimuli with frequency of 1 Hz. Holding potential is –97 mV, and clamp potential is +3 mV, with duration of 200 ms. Only response to the final stimulus is shown. A family of responses is shown in which K_{NaCa} is varied from 0.5 to 2.5 in steps of 0.5 (response for K_{NaCa}=0.25 is also shown), while K_{SR} is held constant at the value accounting for the Ca^{2+} relaxation rate measured in normal myocytes under 0-Na conditions. B, Model NaCa exchange current I_{NaCa} as a function of time in response to the stimuli described in Figure 3A.

with decreasing K_{SR} values, as shown in the data of Figure 3A, as well as Figure 2B (open circles).

Figure 4A shows model cytosolic Ca^{2+} concentration (ordinate, μmol/L) versus time (abscissa, seconds) as K_{NaCa} is varied in steps of 0.5 from 0.5 to 2.5. A plot for K_{NaCa}=0.25 is also shown. K_{SR} is constant at the value estimated using CPA data from normal myocytes (K_{SR}=1.0). Voltage clamp steps from –97 mV to +3 mV with 200 ms duration are applied at a rate of 1.0 Hz. The final Ca^{2+} transient in a sequence of 10 is displayed, with the time origin translated to 0 seconds. There are 3 effects of increased K_{NaCa}. These are (1) increased rate of Ca^{2+} extrusion and lower diastolic Ca^{2+} at the holding potential, (2) reduction in Ca^{2+} transient amplitude in response to the +3 mV voltage-clamp step, and (3) "flattening" of the Ca^{2+} transient during the voltage-clamp step. The increased Ca^{2+} extrusion at the holding potential is a direct consequence of increased NCX activity when the exchanger is operating in the forward mode at the –97-mV holding potential, as shown in Figure 4B. This figure also shows that the NCX operates in reverse mode at the +3 mV clamp potential, thus generating Ca^{2+} influx. The reduction in Ca^{2+} transient amplitude in response to the voltage step is a consequence of the fact that total Ca^{2+} extrusion at the holding potential is greater than total Ca^{2+} influx at the step potential. This produces a smaller Ca^{2+} transient through reductions in SR Ca^{2+} loading and therefore a smaller Ca^{2+}

release. The flattening of the Ca^{2+} transient with increased K_{NaCa} is a direct consequence of increased Ca^{2+} influx during the voltage step, as shown in Figure 4B. Decreased K_{NaCa} values also produce smaller Ca^{2+} transient decay rates, as seen by the data of Figure 4A, as well as Figure 2A (open circles).

Ca^{2+} Transients in Response to Voltage-Clamp Stimuli: Model Versus Experimental Results

Figure 5A shows model Ca^{2+} transients in response to a 1-Hz voltage-clamp pulse train. These transients were computed using K_{SR} and K_{NaCa} parameter values determined from the experimental series in the presence and absence of CPA. The solid line is the normal model Ca^{2+} transient (K_{NaCa}=0.30 and K_{SR}=1.0). The peak Ca^{2+} level (480 nmol/L) agrees well with the value measured experimentally in normal myocytes (450±75 nmol/L).[23] The dotted line is the model Ca^{2+} transient computed using the average K_{NaCa} (0.53) and K_{SR} (0.38) values for failing myocytes. The remaining 2 Ca^{2+} transients (dashed lines) correspond to K_{Naca} and K_{SR} values selected at ±1 SD from the average for failing myocytes. The short dashed line represents parameter choices producing a high degree of SR unloading (large NCX activity, K_{NaCa}=0.60; small SR Ca^{2+} ATPase activity, K_{SR}=0.26). The long-dashed line represents parameter choices that minimize SR unloading (small NCX activity, K_{NaCa}=0.48; large SR Ca^{2+} ATPase activity, K_{SR}=0.51). These data show that as K_{NaCa} is increased from a normal value of 0.30 (taking on values of 0.48, 0.53, and 0.60) and K_{SR} is decreased from the normal value of 1.0 (taking on values 0.51, 0.38, and 0.26), Ca^{2+} transient peak decreases monotonically from the normal value of 480 nmol/L, taking on values of 300, 266, and 230 nmol/L. These values agree well with the average experimental values measured in failing cells of 230±40 nmol/L.[23]

Figure 5B shows a Ca^{2+} transient measured experimentally. The amplitude and waveform of the model predictions in Figure 5A are in close agreement with these experimental data.

Figure 5C shows a plot of the L-type Ca^{2+} current during the Ca^{2+} transients of Figure 5A. The parameter changes have relatively little effect on peak current, but increases in K_{NaCa} or decreases in K_{SR} produce a monotonic increase in the late component of the L-type Ca^{2+} current. As shown in Figure 5D, these same parameter changes also produce monotonic decreases of the subspace Ca^{2+} transient peak. Thus, the increase in the late component of L-type Ca^{2+} current seen in Figure 5C results from a decrease in Ca^{2+}-mediated inactivation of this current due to reductions in magnitude of the subspace Ca^{2+} transient, which is in turn a consequence of reduced SR Ca^{2+} load. As can be appreciated by examining the magnitude of the change in L-type Ca^{2+} current density with alterations in Ca^{2+} handling, this late component of the L-type Ca^{2+} current would be expected to play an important role in determining the action potential plateau. This suggests that in heart failure, alterations in the expression of Ca^{2+} handling proteins that decrease SR Ca^{2+} load and reduce the amplitude of the Ca^{2+} transient may contribute substantially to prolongation of APD by reducing Ca^{2+}-mediated inactivation of the L-type Ca^{2+} current.
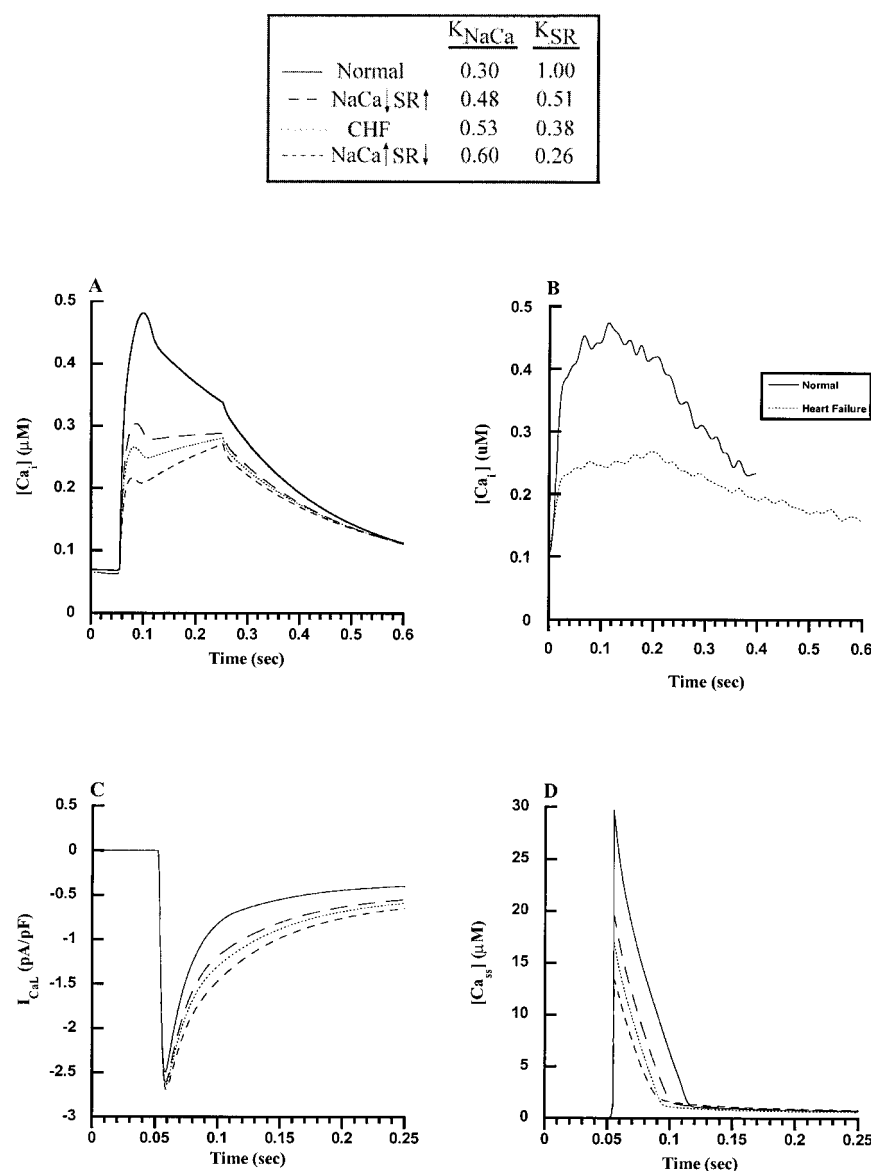
	K_{NaCa}	K_{SR}
—— Normal	0.30	1.00
– – NaCa↓SR↑	0.48	0.51
······· CHF	0.53	0.38
----- NaCa↑SR↓	0.60	0.26

Figure 5. A, Cytosolic Ca^{2+} concentration (μmol/L) as a function of time in response to a 10-second–duration periodic sequence of voltage-clamp stimuli with frequency of 1 Hz. Holding potential is –97 mV, and clamp potential is +3 mV, with duration of 200 ms. Only response to the final stimulus is shown. Results of 4 simulations are shown. Solid line indicates normal model Ca^{2+} transient (K_{NaCa}=0.30; K_{SR}=1.0). Dotted line indicates the average failing model Ca^{2+} transient computed using values of K_{SR} and K_{NaCa} estimated in the presence/absence of CPA, as described in the text (K_{SR}=0.38; K_{NaCa}=0.53). Short-dashed lines show failing model Ca^{2+} transients computed using K_{SR}=0.26 and K_{NaCa}=0.60. Long-dashed lines show failing model Ca^{2+} transients computed using K_{SR}=0.51 and K_{NaCa}=0.48. B, Experimentally measured cytosolic Ca^{2+} concentration (μmol/L) vs time in response to voltage-clamp stimuli (as described in panel A) in normal (solid line) and failing (dotted line) canine ventricular myocytes. C, L-type Ca^{2+} current as a function of time for the stimuli and model parameters described in panel A. D, Subspace Ca^{2+} concentration (μmol/L) as a function of time for the stimuli and model parameters described in panel A.

Discussion

In this article, we present a model of the canine midmyocardial action potential and Ca^{2+} transient. The model is used to estimate the magnitude of SR Ca^{2+} ATPase pump rates and NCX current in normal and failing myocytes[23] using 2 methods. In the first method, model SR Ca^{2+} ATPase current is set to 0, and the NCX current is scaled to yield Ca^{2+} relaxation time constants in response to voltage-clamp stimuli matching those measured experimentally in normal and failing myocytes in the presence of CPA, a blocker of the SR Ca^{2+} ATPase. The extent of functional upregulation of the NCX in heart failure estimated using this approach is in the range of 60% to 100%, with average value 75%. Having constrained the model NCX current, model SR Ca^{2+} ATPase pump current is then estimated by matching the model Ca^{2+} relaxation rate to experimental data obtained in the absence of CPA. Comparison of model SR Ca^{2+} ATPase pump currents estimated for normal and failing myocytes suggests a functional downregulation in heart failure in the range of 49% to 74%, with average value 62%.

In the second method, model NCX current is set to 0, and the SR Ca^{2+} ATPase current is scaled to yield Ca^{2+} relaxation time constants matching those measured experimentally under 0-Na conditions. Functional downregulation of the SR Ca^{2+} ATPase current in heart failure estimated using this approach is in the range of 41% to 54%, with average value 49%. Having constrained the model SR Ca^{2+} ATPase current, NCX current is estimated by matching the model Ca^{2+} relaxation rate to experimental data obtained in control intracellular and extracellular sodium concentrations. Functional NCX upregulation in heart failure estimated using this approach is in the range of 18% to 109%, with average value 38%.

Analysis of protein levels in canine hearts subjected to the tachycardia pacing protocol reveal that both SR Ca^{2+} ATPase and phospholamban proteins are reduced on average by 28%[23] and that NCX protein is increased on average by 104%.[23] Both steady-state mRNA and expressed levels of E-C coupling proteins in failing human ventricular cells have

been measured. The majority of reports agree that there is a $\approx 50\%$ reduction of: (1) mRNA encoding the SR Ca^{2+} ATPase pump,[12–16] (2) expressed SR Ca^{2+} ATPase protein level,[12,17,18] and (3) direct SR Ca^{2+} ATPase uptake rate during heart failure.[19] There is a 55% to 79% increase in Na-Ca exchanger mRNA levels,[12,20] a 36% to 160% increase in expressed protein levels,[12,20–22] and an approximate factor of 2 increase in Na^+/Ca^{2+} exchange activity in human heart failure.[22]

The model-based estimates of functional upregulation and downregulation of the NCX and SR Ca^{2+} ATPase pump reported here are consistent with these reports. Model estimates of average SR Ca^{2+} ATPase functional downregulation are 49% and 62%, depending on the estimation methods used. These values agree well with estimates of mRNA level, protein level, and SR Ca^{2+} ATPase uptake rate measured in human heart failure, but suggest a slightly larger degree of downregulation than indicated by measurements of protein level in canine tachycardia pacing-induced heart failure[23] (28%). Model estimates of average NCX upregulation are 38% and 75%. These estimates agree well with measured increases in mRNA levels in human heart failure and are within the range of variability of measured NCX protein levels in human heart failure. However, the model estimates are slightly lower than is suggested by the increased protein levels measured in the failing canine heart.[23]

Ca^{2+} transients measured in failing human and canine ventricular myocytes exhibit reduced amplitude and slowed relaxation.[5,40–43] Model simulations of Ca^{2+} transients in response to voltage-clamp stimuli reported here demonstrate that the altered expression of the NCX and SR Ca^{2+} ATPase pump measured in failing canine myocytes is sufficient to account for these properties. Both changes contribute to reduced SR Ca^{2+} load and release and therefore reduced amplitude of the early Ca^{2+} transient peak (Figures 3A and 4A). The shape of the Ca^{2+} transient is also controlled by both NCX and SR Ca^{2+} ATPase levels. As the Ca^{2+} ATPase pump is downregulated (Figure 3A), the shape of the plateau portion of the voltage-clamp Ca^{2+} transient changes from negative to 0, then to positive slope. This change in slope is produced by a decrease in early Ca^{2+} release from JSR, which in turn increases the dependence of Ca^{2+} transient shape on Ca^{2+} entry through the L-type Ca^{2+} channel. Upregulation of NCX also influences Ca^{2+} transient shape, tending to flatten the Ca^{2+} transient plateau by increasing reverse-mode Ca^{2+} entry at depolarized potentials (Figure 4A). The interplay between both of these factors accounts for the flattened Ca^{2+} transient shape seen in failing myocytes (Figure 1D, model; Figure 1B, experimental data).

Model Ca^{2+} transients in response to voltage-clamp stimuli exhibit a "knob" at the early peak of the transient (see Figure 3A, for example) that does not appear to be present in the experimental data. This knob disappears as the SR Ca^{2+} level becomes small (Figure 3A), indicating that the knob is dependent on SR Ca^{2+} release. The knob is likely an artifact of model construction. All SR Ca^{2+} release in this model occurs from a single functional unit, defined as a set of L-type Ca^{2+} channels, RyR channels, and the subspace within which they interact. Stern has referred to such models as common

pool models.[44] The knob reflects a large, single Ca^{2+} release event from this single functional unit. In contrast, real cardiac cells have a large number of functional units in which there is local control of calcium-induced calcium release. We have recently implemented a local control model of Ca^{2+} release consisting of an ensemble of functional units, in which each functional unit is defined as an L-type Ca^{2+} channel interacting with a small set of RyR channels through a diadic space. Both L-type Ca^{2+} channels and RyR channels are modeled stochastically using the channel models presented in Jafri et al.[24] In such a model, the stochastic nature of RyR channel openings produces a variable latency of Ca^{2+} release in each functional unit. The Ca^{2+} transients computed using this model exhibit the property of gradedness and do not exhibit the knob seen in Figure 3A due to temporal smearing of Ca^{2+} release times.

A recent study has put forth the hypothesis that coupling between L-type Ca^{2+} channels and RyR channels may be altered in heart failure and that this altered coupling leads to a reduction in amplitude of the Ca^{2+} transient.[45] The results presented here cannot refute this hypothesis. Indeed, structurally detailed models of RyR channel and L-type Ca^{2+} channel interactions in the diadic space predict a strong dependence of these interactions on geometric factors.[46–48] However, the results reported here indicate that such an assumption is not necessary to account for reduced amplitude of Ca^{2+} transients in failing myocytes. Rather, these simulations indicate that the altered expression of Ca^{2+} handling proteins reported by several different groups in both failing human and canine myocytes could account for changes in Ca^{2+} transient amplitude and shape.

The data of Figure 1 demonstrate that downregulation of the outward repolarizing currents I_{K1} and I_{to1}, together with altered expression of the NCX and SR Ca^{2+} ATPase pump, can account for differences in both action potential and Ca^{2+} transient shape in heart failure. However, the data of Figure 1C also indicate that downregulation of I_{K1} and I_{to1}, at least to the extent measured on average in failing cells, has a small effect on APD. Instead, altered expression of Ca^{2+} handling proteins plays a significant role in APD prolongation.

It is not surprising that downregulation of model I_{K1} has only a modest impact on APD, as I_{K1} is primarily responsible for the terminal phase of repolarization. However, the finding that reduction of model I_{to1} has only a small effect on APD differs from the experimental results of Kääb et al[5] in dog myocytes and of Beuckelmann et al[9] in human cells. These experiments were performed using EGTA as an intracellular Ca^{2+} buffer. This buffering minimizes the modulatory effects of Ca^{2+} and thus enhances the relative influence of outward K currents on action potential characteristics. When effects of EGTA buffering are simulated in the model described in this article, block of I_{to1} has a greater influence on APD. An example is shown in Figure 6. The Ca^{2+} buffering effects of EGTA were modeled using the fast buffering approximation developed by Wagner and Keizer,[49] with EGTA= 10 mmol/L and the dissociation constant K_m=0.15 μmol/L. Block of I_{to1} by 95% increases APD_{90} by 73 ms, or $\approx 25\%$ of the control value. These results again emphasize the important modula-
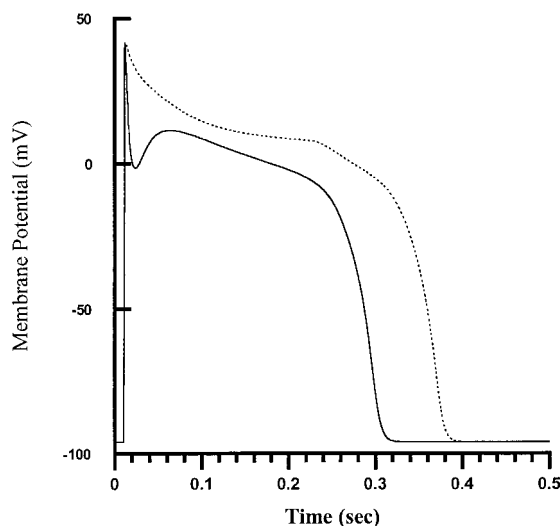
Figure 6. Membrane potential as a function of time for the normal model (solid line) and for the model with a 95% reduction in magnitude of I_{to1} (dotted line). Simulations are done in the presence of EGTA (10 mmol/L; K_m=0.15 μmol/L), using the fast buffering approximation of Wagner and Keizer.[49] Response to fifth stimulus at a cycle length of 1200 ms is shown.

tory role of Ca^{2+} on action potential characteristics in the canine myocyte.

It is also possible that 4-AP block of K currents other than I_{to1} occurred in the Kääb et al[5] experiments, but that such effects were not resolvable. Steady-state current-voltage relations were measured in the presence and absence of 4-AP to assess whether or not this was the case. Data are shown in Figure 10C of Kääb et al[5] and indicate that experimental variability in steady-state current at 0 mV (a potential near that of the action potential plateau) is roughly ±1.0 pA/pF. The sum of model outward currents I_{to1}, I_{K1}, I_{Kr}, and I_{Ks} during the plateau is comparable with the magnitude of this variability in the experimental measurements ($\approx$1.0 pA/pF). Genetic approaches for selective suppression of I_{to1}[50,51] may turn out to be more useful than pharmacological approaches in determining the influence of this current on APD.

The model predicts that one important mechanism of APD prolongation in heart failure is that shown in Figures 1 and 5. Under conditions of reduced SR Ca^{2+} release, there is less Ca^{2+}-mediated inactivation of the L-type Ca^{2+} current. The resulting increase of inward current, as shown for voltage-clamp stimuli in Figure 5C and for action potentials in Figure 1E, helps to maintain and prolong the plateau phase of the action potential. Investigation into the relative contribution of the various Ca^{2+}-regulatory mechanisms and Ca^{2+}-dependent membrane currents in determining the action potential shape and duration is an important area for future experimental and modeling studies.

Appendix

Standard Units (Unless Otherwise Noted) Used in the Following Set of Equations

Quantity	Units
Membrane potential	mV
Membrane current	$\mu A\mu F^{-1}$
Membrane conductance	$mS\mu F^{-1}$
Ionic flux	$mMms^{-1}$
Concentration	mM
Time constant	ms
Rate constant	ms^{-1}

Membrane Currents

Na^+ Current I_{Na}

$$(A.1) \qquad I_{Na} = \bar{G}_{Na} m^3 h j (V - E_{Na})$$

$$(A.2) \qquad E_{Na} = \frac{RT}{F} \ln\left(\frac{[Na^+]_o}{[Na^+]_i}\right)$$

$$(A.3) \qquad \frac{dm}{dt} = \alpha_m(1-m) - \beta_m m$$

$$(A.4) \qquad \frac{dh}{dt} = \alpha_h(1-h) - \beta_h h$$

$$(A.5) \qquad \frac{dj}{dt} = \alpha_j(1-j) - \beta_j j$$

$$(A.6) \qquad \alpha_m = 0.32 \frac{V+47.13}{1-e^{-0.1(V+47.13)}}$$

$$(A.7) \qquad \beta_m = 0.08 e^{\frac{-V}{11}}$$

For $V \geq -40$ mV,

$$(A.8) \qquad \alpha_h = 0.0$$

$$(A.9) \qquad \beta_h = \frac{1}{0.13(1+e^{(V+10.66)/-11.1})}$$

$$(A.10) \qquad \alpha_j = 0.0$$

$$(A.11) \qquad \beta_j = 0.3 \frac{e^{-2.535 \times 10^{-7} V}}{1+e^{-0.1(V+32)}}$$

For $V < -40$ mV,

$$(A.12) \qquad \alpha_h = 0.135 e^{(80+V)/-6.8}$$

$$(A.13) \qquad \beta_h = 3.56 e^{0.079V} + 3.1 \times 10^5 e^{0.35V}$$

$$(A.14) \qquad \alpha_j = (-127140 e^{0.2444V} - 3.474$$
$$\times 10^{-5} e^{-0.04391V}) \frac{V+37.78}{1+e^{0.311(V+79.23)}}$$

$$(A.15) \qquad \beta_j = 0.1212 \frac{e^{-0.01052V}}{1+e^{-0.1378(V+40.14)}}$$

Rapid-Activating Delayed Rectifier K^+ Current I_{Kr}

$$(A.16) \qquad I_{Kr} = \bar{G}_{Kr} f([K^+]_o) R(V) X_{Kr} (V - E_K)$$

(A.17)
$$E_K = \frac{RT}{F}\ln\left(\frac{[K^+]_o}{[K^+]_i}\right)$$

(A.18)
$$R(V) = \frac{1}{1 + 1.4945e^{0.0446V}}$$

(A.19)
$$f([K^+]_o) = \sqrt{[K^+]_o/4}$$

(A.20)
$$\frac{dX_{Kr}}{dt} = K_{12}(1 - X_{Kr}) - K_{21}X_{Kr}$$

(A.21)
$$K_{12} = e^{-5.495 + 0.1691V}$$

(A.22)
$$K_{21} = e^{-7.677 - 0.0128V}$$

Slow-Activating Delayed Rectifier K^+ Current I_{Ks}

(A.23)
$$I_{Ks} = \bar{G}_{Ks}X_{Ks}^2(V - E_{Ks})$$

(A.24)
$$E_{Ks} = \frac{RT}{F}\ln\left(\frac{[K^+]_o + 0.01833[Na^+]_o}{[K^+]_i + 0.01833[Na^+]_i}\right)$$

(A.25)
$$\frac{dX_{Ks}}{dt} = (X_{Ks}^\infty - X_{Ks})/\tau_{X_{Ks}}$$

(A.26)
$$X_{Ks}^\infty = \frac{1}{1 + e^{-(V - 24.7)/13.6}}$$

(A.27)
$$\tau_{X_{Ks}} = \frac{1}{\frac{0.0000719(V-10)}{1 - e^{-0.148(V-10)}} + \frac{0.000131(V-10)}{e^{0.0687(V-10)} - 1}}$$

Transient Outward K^+ Current I_{to1}

(A.28)
$$I_{to1} = \bar{G}_{to1}X_{to1}Y_{to1}(V - E_K)$$

(A.29)
$$\frac{dX_{to1}}{dt} = \alpha_{X_{to1}}(1 - X_{to1}) - \beta_{X_{to1}}X_{to1}$$

(A.30)
$$\frac{dY_{to1}}{dt} = \alpha_{Y_{to1}}(1 - Y_{to1}) - \beta_{Y_{to1}}Y_{to1}$$

(A.31)
$$\alpha_{X_{to1}} = 0.04516e^{0.03577V}$$

(A.32)
$$\beta_{X_{to1}} = 0.0989e^{-0.06237V}$$

(A.33)
$$\alpha_{Y_{to1}} = \frac{0.005415e^{-(V+33.5)/5}}{1 + 0.051335e^{-(V+33.5)/5}}$$

(A.34)
$$\beta_{Y_{to1}} = \frac{0.005415e^{(V+33.5)/5}}{1 + 0.051335e^{(V+33.5)/5}}$$

Time-Independent K^+ Current I_{K_1}

(A.35)
$$I_{K_1} = \bar{G}_{K_1}K_1^\infty(V)\left(\frac{[K^+]_o}{[K^+]_o + K_{mK1}}\right)(V - E_K)$$

(A.36)
$$K_1^\infty(V) = \frac{1}{2 + e^{1.5\frac{F}{RT}(V - E_K)}}$$

Plateau K^+ Current I_{Kp}

(A.37)
$$I_{Kp} = \bar{G}_{Kp}K_p(V)(V - E_K)$$

(A.38)
$$K_p(V) = \frac{1}{1 + e^{(7.488 - V)/5.98}}$$

NCX Current I_{NaCa}

(A.39)
$$I_{NaCa} = k_{NaCa}\frac{5000}{K_{m,Na}^3 + [Na^+]_o^3}\frac{1}{K_{m,Ca} + [Ca^{2+}]_o}\frac{1}{1 + k_{sat}e^{(\eta-1)VF/RT}}$$
$$(e^{\eta VF/RT} \times [Na^+]_i^3[Ca^{2+}]_o - e^{(\eta-1)VF/RT}[Na^+]_o^3[Ca^{2+}]_i)$$

Na^+-K^+ Pump Current I_{NaK}

(A.40)
$$I_{NaK} = \bar{I}_{NaK}f_{NaK}\frac{1}{1 + \left(\frac{K_{m,Nai}}{[Na^+]_i}\right)^{1.5}}\frac{[K^+]_o}{[K^+]_o + K_{m,Ko}}$$

(A.41)
$$f_{NaK} = \frac{1}{1 + 0.1245e^{-0.1VF/RT} + 0.0365\sigma e^{-VF/RT}}$$

(A.42)
$$\sigma = \frac{1}{7}(e^{\frac{[Na^+]_o}{67.3}} - 1)$$

Sarcolemmal Ca^{2+} Pump Current $I_{p(Ca)}$

(A.43)
$$I_{p(Ca)} = \bar{I}_{p(Ca)}\frac{[Ca^{2+}]_i}{K_{m,p(Ca)} + [Ca^{2+}]_i}$$

Ca^{2+} Background Current $I_{Ca,b}$

(A.44)
$$I_{Ca,b} = \bar{G}_{Ca,b}(V - E_{Ca})$$

(A.45)
$$E_{Ca} = \frac{RT}{2F}\ln\left(\frac{[Ca^{2+}]_o}{[Ca^{2+}]_i}\right)$$

Na^+ Background Current $I_{Na,b}$

(A.46)
$$I_{Na,b} = \bar{G}_{Na,b}(V - E_{Na})$$

Membrane Potential

(A.47)
$$\frac{dV}{dt} = -(I_{Na} + I_{Ca} + I_{Ca,K} + I_{Kr} + I_{Ks} + I_{to1} + I_{K_1} + I_{Kp} + I_{NaCa}$$
$$+ I_{NaK} + I_{p(Ca)} + I_{Ca,b} + I_{Na,b})$$

Ca^{2+} Handling Mechanisms

L-Type Ca^{2+} Current I_{Ca}

(A.48)
$$\alpha = 0.4e^{(V+2)/10}$$

(A.49)
$$\beta = 0.05e^{-(V+2)/13}$$

(A.50)
$$\alpha' = \alpha a$$

(A.51)
$$\beta' = \frac{\beta}{b}$$

(A.52)
$$\gamma = 0.10375[Ca^{2+}]_{ss}$$

(A.53)
$$\frac{dC_0}{dt} = \beta C_1 + \omega C_{Ca0} - (4\alpha + \gamma)C_0$$

(A.54)
$$\frac{dC_1}{dt} = 4\alpha C_0 + 2\beta C_2 + \frac{\omega}{b}C_{Ca1}$$
$$- (\beta + 3\alpha + \gamma a)C_1$$

(A.55)
$$\frac{dC_2}{dt} = 3\alpha C_1 + 3\beta C_3 + \frac{\omega}{b^2}C_{Ca2}$$
$$- (2\beta + 2\alpha + \gamma a^2)C_2$$

(A.56)
$$\frac{dC_3}{dt} = 2\alpha C_2 + 4\beta C_4 + \frac{\omega}{b^3}C_{Ca3}$$
$$- (3\beta + \alpha + \gamma a^3)C_3$$

(A.57)
$$\frac{dC_4}{dt} = \alpha C_3 + gO + \frac{\omega}{b^4}C_{Ca4}$$
$$- (4\beta + f + \gamma a^4)C_4$$

(A.58)
$$\frac{dO}{dt} = fC_4 - gO$$

(A.59)
$$\frac{dC_{Ca0}}{dt} = \beta' C_{Ca1} + \gamma C_0 - (4\alpha' + \omega)C_{Ca0}$$

(A.60)
$$\frac{dC_{Ca1}}{dt} = 4\alpha' C_{Ca0} + 2\beta' C_{Ca2} + \gamma aC_1$$
$$- \left(\beta' + 3\alpha' + \frac{\omega}{b}\right)C_{Ca1}$$

(A.61)
$$\frac{dC_{Ca2}}{dt} = 3\alpha' C_{Ca1} + 3\beta' C_{Ca3} + \gamma a^2 C_2$$
$$- \left(2\beta' + 2\alpha' + \frac{\omega}{b^2}\right)C_{Ca2}$$

(A.62)
$$\frac{dC_{Ca3}}{dt} = 2\alpha' C_{Ca2} + 4\beta' C_{Ca4} + \gamma a^3 C_3$$
$$- \left(3\beta' + \alpha' + \frac{\omega}{b^3}\right)C_{Ca3}$$

(A.63)
$$\frac{dC_{Ca4}}{dt} = \alpha' C_{Ca3} + g' O_{Ca} + \gamma a^4 C_4$$
$$- \left(4\beta' + f' + \frac{\omega}{b^4}\right)C_{Ca4}$$

(A.64)
$$\frac{dO_{Ca}}{dt} = f' C_{Ca4} - g' O_{Ca}$$

(A.65)
$$\bar{I}_{Ca} = \frac{\bar{P}_{Ca}}{C_{sc}}\frac{4VF^2}{RT}\frac{0.001e^{2VF/RT} - 0.341[Ca^{2+}]_o}{e^{2VF/RT} - 1}$$

(A.66)
$$I_{Ca} = \bar{I}_{Ca}y\{O + O_{Ca}\}$$

(A.67)
$$I_{Ca,K} = \frac{P'_K}{C_{sc}}y\{O + O_{Ca}\}$$
$$\frac{VF^2}{RT}\frac{[K^+]_i e^{VF/RT} - [K^+]_o}{e^{VF/RT} - 1}$$

(A.68)
$$P'_K = \frac{\bar{P}_K}{1 + \frac{\bar{I}_{Ca}}{I_{Ca_{half}}}}$$

(A.69)
$$\frac{dy}{dt} = \frac{y_\infty - y}{\tau_y}$$

(A.70)
$$y_\infty = \frac{0.8}{1 + e^{(V+12.5)/5}} + 0.2$$

(A.71)
$$\tau_y = 20 + \frac{600}{1 + e^{(V+20)/9.5}}$$

RyR Channel (Keizer and Levine)[27]

(A.72)
$$\frac{dP_{C_1}}{dt} = -k_a^+[Ca^{2+}]_{ss}^n P_{C_1} + k_a^- P_{O_1}$$

(A.73)
$$\frac{dP_{O_1}}{dt} = k_a^+[Ca^{2+}]_{ss}^n P_{C_1} - k_a^- P_{O_1} - k_b^+[Ca^{2+}]_{ss}^m P_{O_1}$$
$$+ k_b^- P_{O_2} - k_c^+ P_{O_1} + k_c^- P_{C_2}$$

(A.74)
$$\frac{dP_{O_2}}{dt} = k_b^+[Ca^{2+}]_{ss}^m P_{O_1} - k_b^- P_{O_2}$$

(A.75)
$$\frac{dP_{C_2}}{dt} = k_c^+ P_{O_1} - k_c^- P_{C_2}$$

(A.76)
$$J_{rel} = v_1(P_{O_1} + P_{O_2})([Ca^{2+}]_{JSR} - [Ca^{2+}]_{ss})$$

SERCA2a Pump (Shannon et al)[38]

(A.77)
$$f_b = ([Ca^{2+}]_i/K_{fb})^{N_{fb}}$$

(A.78)
$$r_b = ([Ca^{2+}]_{NSR}/K_{rb})^{N_{rb}}$$

(A.79)
$$J_{up} = K_{SR}\frac{v_{maxf}f_b - v_{maxr}r_b}{1 + f_b + r_b}$$

Intracellular Ca²⁺ Fluxes

(A.80)
$$J_{tr} = \frac{[Ca^{2+}]_{NSR} - [Ca^{2+}]_{JSR}}{\tau_{tr}}$$

(A.81)
$$J_{xfer} = \frac{[Ca^{2+}]_{ss} - [Ca^{2+}]_i}{\tau_{xfer}}$$

(A.82)
$$J_{trpn} = \frac{d[HTRPNCa]}{dt} + \frac{d[LTRPNCa]}{dt}$$

(A.83)
$$\frac{d[HTRPNCa]}{dt} = k_{htrpn}^+[Ca^{2+}]_i([HTRPN]_{tot} - [HTRPNCa])$$
$$- k_{htrpn}^-[HTRPNCa]$$

(A.84)
$$\frac{d[LTRPNCa]}{dt} = k_{ltrpn}^+[Ca^{2+}]_i([LTRPN]_{tot} - [LTRPNCa])$$
$$- k_{ltrpn}^-[LTRPNCa]$$

Intracellular Ion Concentrations

(A.85)
$$\frac{d[Na^+]_i}{dt} = -(I_{Na} + I_{Na,b} + 3I_{NaCa} + 3I_{NaK})\frac{A_{cap}C_{sc}}{V_{myo}F}$$

(A.86)
$$\frac{d[K^+]_i}{dt} = -(I_{Kr} + I_{Ks} + I_{to1} + I_{K1} + I_{Kp} + I_{Ca,K}$$
$$- 2I_{NaK})\frac{A_{cap}C_{sc}}{V_{myo}F}$$

(A.87)
$$\frac{d[Ca^{2+}]_i}{dt} = \beta_i\left\{J_{xfer} - J_{up} - J_{trpn} - (I_{Ca,b} - 2I_{NaCa} + I_{p(Ca)})\frac{A_{cap}C_{sc}}{2V_{myo}F}\right\}$$

(A.88)
$$\beta_i = \left\{1 + \frac{[CMDN]_{tot}K_m^{CMDN}}{(K_m^{CMDN} + [Ca^{2+}]_i)^2}\right\}^{-1}$$

(A.89)
$$\beta_{ss} = \left\{1 + \frac{[CMDN]_{tot}K_m^{CMDN}}{(K_m^{CMDN} + [Ca^{2+}]_{ss})^2}\right\}^{-1}$$

(A.90)
$$\beta_{JSR} = \left\{1 + \frac{[CSQN]_{tot}K_m^{CSQN}}{(K_m^{CSQN} + [Ca^{2+}]_{JSR})^2}\right\}^{-1}$$

(A.91)
$$\frac{d[Ca^{2+}]_{ss}}{dt} = \beta_{ss}\left\{J_{rel}\frac{V_{JSR}}{V_{ss}} - J_{xfer}\frac{V_{myo}}{V_{ss}} - (I_{Ca})\frac{A_{cap}C_{sc}}{2V_{ss}F}\right\}$$

(A.92)
$$\frac{d[\text{Ca}^{2+}]_{\text{JSR}}}{dt} = \beta_{\text{JSR}}\{J_{\text{tr}} - J_{\text{rel}}\}$$

(A.93)
$$\frac{d[\text{Ca}^{2+}]_{\text{NSR}}}{dt} = J_{\text{up}}\frac{V_{\text{myo}}}{V_{\text{NSR}}} - J_{\text{tr}}\frac{V_{\text{JSR}}}{V_{\text{NSR}}}$$

Tables

TABLE 1.   Cell Geometry Parameters

Parameter	Definition	Value
C_{sc}	Specific membrane capacity	1.00 μF cm^{-2}
A_{cap}	Capacitive membrane area	1.534$\times$10^{-4}cm^2
V_{myo}	Myoplasmic volume	25.84$\times$10^{-6} μL
V_{JSR}	JSR volume	0.16$\times$10^{-6} μL
V_{NSR}	NSR volume	2.10$\times$10^{-6} μL
V_{SS}	Subspace volume	1.2$\times$10^{-9} μL

TABLE 2.   Standard Ionic Concentrations

Parameter	Definition	Value
$[\text{K}^+]_o$	Extracellular K$^+$ concentration	4.0 mmol/L
$[\text{Na}^+]_o$	Extracellular Na$^+$ concentration	138.0 mmol/L
$[\text{Ca}^{2+}]_o$	Extracellular Ca^{2+} concentration	2.0 mmol/L

TABLE 3.   Membrane Current Parameters

Parameter	Definition	Value
F	Faraday constant	96.5 coulomb mmol^{-1}
T	Absolute temperature	310 K
R	Ideal gas constant	8.314 Jmol^{-1}K^{-1}
$\bar{G}_{\text{Kr}}$	Peak I$_{\text{Kr}}$ conductance	0.0034 mSμF^{-1}
$\bar{G}_{\text{Ks}}$	Peak I$_{\text{Ks}}$ conductance	0.00271 mSμF^{-1}
$\bar{G}_{\text{to1}}$	Peak I$_{\text{to1}}$ conductance	0.23815 mSμF^{-1}
$\bar{G}_{\text{K1}}$	Peak I$_{\text{K1}}$ conductance	2.8 mSμF^{-1}
$\bar{G}_{\text{Kp}}$	Peak I$_{\text{Kp}}$ conductance	0.002216 mSμF^{-1}
$\bar{G}_{\text{Na}}$	Peak I$_{\text{Na}}$ conductance	12.8 mSμF^{-1}
k_{NaCa}	Scaling factor of Na$^+$-Ca^{2+} exchange	0.30 μAμF^{-1}
K_{mNa}	Na$^+$ half-saturation constant for Na$^+$-Ca^{2+} exchange	87.5 mmol/L
K_{mCa}	Ca^{2+} half-saturation constant for Na$^+$-Ca^{2+} exchange	1.38 mmol/L
K_{mK1}	Ca^{2+} half-saturation constant for I$_{\text{K1}}$	13.0 mmol/L
k_{sat}	Na$^+$-Ca^{2+} exchange sat. factor at negative potentials	0.2
η	Controls voltage dependence of Na$^+$-Ca^{2+} exchange	0.35
$\bar{I}_{\text{NaK}}$	Maximum Na$^+$-K$^+$ pump current	0.693 μAμF^{-1}
$K_{\text{m,Nai}}$	Na$^+$ half-saturation constant for Na$^+$-K$^+$ pump	10.0 mmol/L
$K_{\text{m,Ko}}$	K$^+$ half-saturation constant for Na$^+$-K$^+$ pump	1.5 mmol/L
$\bar{I}_{\text{p(Ca)}}$	Maximum sarcolemmal Ca^{2+} pump current	0.05 μAμF^{-1}
$K_{\text{m,p(Ca)}}$	Half-saturation constant for sarcolemmal Ca^{2+} pump	0.00005 mmol/L
$\bar{G}_{\text{Ca,b}}$	Maximum background Ca^{2+} current conductance	0.0003842 mSμF^{-1}
$\bar{G}_{\text{Na,b}}$	Maximum background Na$^+$ current conductance	0.0031 mSμF^{-1}

TABLE 4. SR Parameters

Parameter	Definition	Value
v_1	Maximum RyR channel Ca^{2+} flux	1.8 ms^{-1}
K_{fb}	Forward half-saturation constant for Ca^{2+} ATPase	0.168×10^{-3} mmol/L
K_{rb}	Backward half-saturation constant for Ca^{2+} ATPase	3.29 mmol/L
K_{SR}	Scaling factor for Ca^{2+} ATPase	1.0
N_{fb}	Forward cooperativity constant for Ca^{2+} ATPase	1.2
N_{rb}	Reverse cooperativity constant for Ca^{2+} ATPase	1.0
v_{maxf}	Ca^{2+} ATPase forward rate parameter	0.813×10^{-4} mmol/L ms^{-1}
v_{maxr}	Ca^{2+} ATPase reverse rate parameter	0.318×10^{-3} mmol/L ms^{-1}
τ_{tr}	Time constant for transfer from NSR to JSR	0.5747 ms
τ_{xfer}	Time constant from subspace to myoplasm	26.7 ms
k_a^+	RyR $P_{C_1} - P_{O_1}$ rate constant	12.15×10^9 mmol/L^{-4} ms^{-1}
k_a^-	RyR $P_{O_1} - P_{C_1}$ rate constant	0.576 ms^{-1}
k_b^+	RyR $P_{O_1} - P_{O_2}$ rate constant	4.05×10^6 mmol/L^{-3} ms^{-1}
k_b^-	RyR $P_{O_2} - P_{O_1}$ rate constant	1.930 ms^{-1}
k_c^+	RyR $P_{O_1} - P_{C_2}$ rate constant	0.100 ms^{-1}
k_c^-	RyR $P_{C_2} - P_{O_1}$ rate constant	0.0008 ms^{-1}
n	RyR Ca^{2+} cooperativity parameter $P_{C_1} - P_{O_1}$	4
m	RyR Ca^{2+} cooperativity parameter $P_{O_1} - P_{O_2}$	3

TABLE 5. L-Type Ca^{2+} Channel Parameters

Parameter	Definition	Value
f	Transition rate into open state	0.3 ms^{-1}
g	Transition rate out of open state	2.0 ms^{-1}
f'	Transition rate into open state for mode Ca	0.005 ms^{-1}
g'	Transition rate out of open state for mode Ca	7.0 ms^{-1}
b	Mode transition parameter	2.0
a	Mode transition parameter	2.0
ω	Mode transition parameter	0.01 ms^{-1}
$\bar{P}_{Ca}$	L-type Ca^{2+} channel permeability to Ca^{2+}	$3.125\ 10^{-4}$ cm s^{-1}
$\bar{P}_K$	L-type Ca^{2+} channel permeability to K^+	$5.79\ 10^{-7}$ cm s^{-1}
$I_{Ca_{half}}$	$\bar{I}_{Ca}$ level that reduces P'_K by half	-0.265 $\mu A \mu F^{-1}$

TABLE 6. Buffering Parameters

Parameter	Definition	Value
$[LTRPN]_{tot}$	Total troponin low-affinity site concentration	70.0×10^{-3} mmol/L
$[HTRPN]_{tot}$	Total troponin high-affinity site concentration	140.0×10^{-3} mmol/L
k_{htrpn}^+	Ca^{2+} on rate for troponin high-affinity sites	20.0 mmol/$L^{-1}ms^{-1}$
k_{htrpn}^-	Ca^{2+} off rate for troponin high-affinity sites	66.0×10^{-6} ms^{-1}
k_{ltrpn}^+	Ca^{2+} on rate for troponin low-affinity sites	40.0 mmol/L^{-1} ms^{-1}
k_{ltrpn}^-	Ca^{2+} on rate for troponin low-affinity sites	0.040 ms^{-1}
$[CMDN]_{tot}$	Total myoplasmic calmodulin concentration	50.0×10^{-3} mmol/L
$[CSQN]_{tot}$	Total NSR calsequestrin concentration	15.0 mmol/L
K_m^{CMDN}	Ca^{2+} half-saturation constant for calmodulin	2.38×10^{-3} mmol/L
K_m^{CSQN}	Ca^{2+} half-saturation constant for calsequestrin	0.8 mmol/L

TABLE 7.   State Variable Initial Conditions

Variable	Definition	Initial Value
t	Time	0.00 ms
V	Membrane potential	-95.87 mV
m	I_{Na} activation gate	2.4676×10^{-4}
h	I_{Na} inactivation gate	0.99869
j	I_{Na} slow inactivation gate	0.99887
X_{Kr}	I_{Kr} activation gate	0.6935
X_{Ks}	I_{Ks} activation gate	1.4589×10^{-4}
X_{to1}	I_{to1} activation gate	3.742×10^{-5}
Y_{to1}	I_{to1} inactivation gate	1.00
$[Na^+]_i$	Intracellular Na^+ concentration	10.00 mmol/L
$[K^+]_i$	Intracellular K^+ concentration	159.48 mmol/L
$[Ca^{2+}]_i$	Myoplasmic Ca^{2+} concentration	8.464×10^{-5} mmol/L
$[Ca^{2+}]_{NSR}$	NSR Ca^{2+} concentration	0.2620 mmol/L
$[Ca^{2+}]_{ss}$	Subspace SR Ca^{2+} concentration	1.315×10^{-4} mmol/L
$[Ca^{2+}]_{JSR}$	JSR Ca^{2+} concentration	0.2616 mmol/L
P_{C_1}	Fraction of channels in state P_{C_1}	0.4929
P_{O_1}	Fraction of channels in state P_{O_1}	6.027×10^{-4}
P_{O_2}	Fraction of channels in state P_{O_2}	2.882×10^{-9}
P_{C_2}	Fraction of channels in state P_{C_2}	0.5065
C_0	L-type Ca^{2+} channel closed: mode normal	0.99802
C_1	L-type Ca^{2+} channel closed: mode normal	1.9544×10^{-6}
C_2	L-type Ca^{2+} channel closed: mode normal	0.00
C_3	L-type Ca^{2+} channel closed: mode normal	0.00
C_4	L-type Ca^{2+} channel closed: mode normal	0.00
O	L-type Ca^{2+} channel open: mode normal	0.00
C_{Ca0}	L-type Ca^{2+} channel closed: mode Ca	1.9734×10^{-3}
C_{Ca1}	L-type Ca^{2+} channel closed: mode Ca	0.00
C_{Ca2}	L-type Ca^{2+} channel closed: mode Ca	0.00
C_{Ca3}	L-type Ca^{2+} channel closed: mode Ca	0.00
C_{Ca4}	L-type Ca^{2+} channel closed: mode Ca	0.00
O_{Ca}	L-type Ca^{2+} channel open: mode Ca	0.00
y	I_{Ca} inactivation gate	0.7959
[LTRPNCa]	Concentration of Ca^{2+}-bound low-affinity troponin sites	5.5443×10^{-3} mmol/L
[HTRPNCa]	Concentration of Ca^{2+}-bound high-affinity troponin sites	136.64×10^{-3} mmol/L

References

1. Calderone A, Bouvier M, Li K, Juneau C, de Champlain J, Rouleau J-L. Dysfunction of the β- and α-adrenergic systems in a model of congestive heart failure: the pacing-overdrive dog. *Circ Res*. 1991;69:332–343.
2. Spinale FG, Fulbright M, Mukherjee R, Tanaka R, Hu J, Crawford FA, Zile MR. Relation between ventricular and myocyte function with tachycardia-induced cardiomyopathy. *Circ Res*. 1992;71:174–187.
3. Spinale FG, Holzgrefe HH, Mukherjee R, Arthur SR, Child MJ, Powell JR, Koster WH. LV and myocyte structure and function after early recovery from tachycardia-induced cardiomyopathy. *Am J Physiol*. 1995;268:H836–H847.
4. Kajstura J, Zhang X, Liu Y, Szoke E, Cheng W, Olivetti G, Hintze TH, Anversa P. The cellular basis of pacing-induced dilated cardiomyopathy: myocyte cell loss and myocyte cellular reactive hypertrophy. *Circulation*. 1995;92:2306–2317.
5. Kääb S, Nuss HB, Chiamvimonvat N, O'Rourke B, Pak PH, Kass DA, Marbán E, Tomaselli GF. Ionic mechanism of action potential prolongation in ventricular myocytes from dogs with pacing-induced heart failure. *Circ Res*. 1996;78:262–273.
6. Cory CR, McCutcheon LJ, O'Grady M, Pang AW, Geiger JD, O'Brien PJ. Compensatory downregulation of myocardial Ca channel in SR from dogs with heart failure. *Am J Physiol*. 1993;264:H926–H937.
7. Williams RE, Kass DA, Kawagoe Y, Pak P, Tunin RS, Shah R, Hwang A, Feldman AM. Endomyocardial gene expression during development

of pacing tachycardia-induced heart failure in the dog. *Circ Res*. 1994; 75:615–623.

8. Kim CH, Fan T-HM, Kelly PF, Himura Y, Delehanty JM, Hang C-L, Liang C-S. Isoform-specific regulation of myocardial Na, K-ATPase α-subunit in congestive heart failure. *Circulation*. 1994;89:313–320.

9. Beuckelmann DJ, Nabauer M, Erdmann E. Alterations of K^+ currents in isolated human ventricular myocytes from patients with terminal heart failure. *Circ Res*. 1993;73:379–385.

10. Koumi S-I, Backer CL, Arentzen CE. Characterization of inwardly rectifying K+ channel in human cardiac myocytes: Alterations in channel behavior in myocytes isolated from patients with idiopathic dilated cardiomyopathy. *Circulation*. 1995;92:164–174.

11. Nabauer M, Beuckelmann DJ, Uberfuhr P, Steinbeck G. Regional differences in current density and rate-dependent properties of the transient outward current in subepicardial and subendocardial myocytes of human left ventricle. *Circulation*. 1996;93:168–177.

12. Studer R, Reinecke H, Bilger J, Eschenhagen T, Bohm M, Hasenfuss G, Just H, Holtz J, Drexler H. Gene expression of the cardiac Na-Ca exchanger in end-stage human heart failure. *Circ Res*. 1994;75:443–453.

13. Mercadier J-J, Lompre A-M, Duc P, Boheler KR, Fraysse J-B, Wisnewsky C, Allen PD, Komajda M, Schwartz K. Altered sarcoplasmic reticulum Ca2+-ATPase gene expression in the human ventricle during end-stage heart failure. *J Clin Invest*. 1990;85:305–309.

14. Takahashi T, Allen PD, Lacro RV, Marks AR, Dennis AR, Schoen FJ, Grossman W, Marsh JD, Izumo S. Expression of dihydropyridine receptor (Ca2+ channel) and calsequestrin genes in the myocardium of patients with end-stage heart failure. *J Clin Invest*. 1992;90:927–935.

15. Arai M, Alpert NR, MacLennan DH, Barton P, Periasamy M. Alterations in sarcoplasmic reticulum gene expression in human heart failure: a possible mechanism for alterations in systolic and diastolic properties of the failing myocardium. *Circ Res*. 1993;72:463–469.

16. Movsesian MA, Bristow MR, Krall J. Ca uptake by cardiac sarcoplasmic reticulum from patients with idiopathic dilated cardiomyopathy. *Circ Res*. 1989;65:1141–1144.

17. Meyer M, Schillinger W, Pieske B, Holubarsch C, Heilmann C, Posival H, Kuwajima G, Mikoshiba K, Just H, Hasenfuss G. Alterations of sarcoplasmic reticulum proteins in failing human dilated cardiomyopathy. *Circulation*. 1995;92:778–784.

18. Hasenfuss G, Reinecke H, Studer R, Meyer M, Pieske B, Holtz J, Holubarsch C, Posival H, Just H, Drexler H. Relation between myocardial function and expression of sarcoplasmic reticulum Ca-ATPase in failing and nonfailing human myocardium. *Circ Res*. 1994;75:434–442.

19. Limas CJ, Olivari M-T, Goldenberg IF, Levine TB, Benditt DG, Simon A. Calcium uptake by cardiac sarcoplasmic reticulum in human dilated cardiomyopathy. *Cardiovasc Res*. 1987;21:601–605.

20. Flesch M, Schwinger RH, Schiffer F, Frank K, Sudkamp M, Kuhn-Regnier F, Arnold G. Evidence for functional relevance of an enhanced expression of the Na^+-Ca^{2+} exchanger in failing human myocardium. *Circulation*. 1996;94:992–1002.

21. Reinecke H, Studer R, Vetter R, Just H, Holtz J, Drexler H. Role of the cardiac sarcolemmal Na+-Ca2+ exchanger in end-stage human heart failure. *Ann N Y Acad Sci*. 1996;779:543–545.

22. Reinecke H, Studer R, Vetter R, Holtz J, Drexler H. Cardiac Na/Ca exchange activity in patients with end-stage heart failure. *Cardiovasc Res*. 1996;31:48–54.

23. O'Rourke B, Kass DA, Tomaselli GF, Kääb S, Tunin R, Marbán E. Mechanisms of altered excitation-contraction coupling in canine tachycardia-induced heart failure, I: experimental studies. *Circ Res*. 1999; 84:562–570.

24. Jafri S, Rice JJ, Winslow RL. Cardiac Ca^{2+} dynamics: the roles of ryanodine receptor adaptation and sarcoplasmic reticulum load. *Biophys J*. 1998;74:1149–1168.

25. Luo CH, Rudy Y. A dynamic model of the cardiac ventricular action potential, I: simulations of ionic currents and concentration changes. *Circ Res*. 1994;74:1071–1096.

26. Imredy JP, Yue DT. Mechanism of Ca^{2+}-sensitive inactivation of L-type Ca^{2+} channels. *Neuron*. 1994;12:1301–1318.

27. Keizer J, Levine L. Ryanodine receptor adaptation and Ca^{2+}-induced Ca^{2+} release-dependent Ca^{2+} oscillations. *Biophys J*. 1996;71:3477–3487.

28. Liu D-W, Gintant GA, Antzelevitch C. Ionic basis for electrophysiological distinctions among epicardial, midmyocardial, and endocardial myocytes from the free wall of the canine left ventricle. *Circulation*. 1993;72:671–687.

29. Tseng GN, Hoffman BF. Two components of transient outward current in canine ventricular myocytes. *Circ Res*. 1989;64:633–647.

30. Zygmunt AC. Intracellular calcium activates a chloride current in canine ventricular myocytes. *Am J Physiol*. 1994;267:H1984–H1995.

31. Campbell DL, Rasmusson RL, Strauss HC. The calcium-independent transient outward potassium current in isolated ferret right ventricular myocytes. I. Basic characterization and kinetic analysis. *J Gen Physiol*. 1993;101:571–601.

32. Zeng J, Laurita KR, Rosenbaum DS, Rudy Y. Two components of the delayed rectifier K^+ current in ventricular myocytes of the guinea pig type. *Circ Res*. 1995;77:140–152.

33. Liu DW, Antzelevitch C. Characteristics of the delayed rectifier current (I_{kr} and I_{ks}) in canine ventricular epicardial, midmyocardial, and endocardial cells: a weaker I_{ks} contributes to the longer action potential of the M cell. *Circ Res*. 1995;76:351–365.

34. Gintant GA. Regional differences in I_k density in canine left ventricle: role of I_{ks} in electrical heterogeneity. *Am J Physiol*. 1995;268: H604–H613.

35. Gintant GA. Two components of delayed rectifier current in canine atrium and ventricle: does I_{ks} play a role in the reverse rate dependence of class III agents? *Circ Res*. 1996;78:26–37.

36. Deleted in proof.

37. Tseng G-N, Robinson RB, Hoffman BF. Passive properties and membrane currents of canine ventricular myocytes. *J Gen Physiol*. 1987; 90:671–701.

38. Shannon TR, Ginsburg KS, Bers DM. Reverse mode of the SR Ca pump limits SR Ca uptake in permeabilized and voltage clamped myocytes. In: Johnson RG, Kranias EG, Hasselbach W, eds. *Cardiac Sarcoplasmic Reticulum Function and Regulation of Contractility*. Washington, DC: New York Academy of Sciences; 1998;853:350–356.

39. Shannon TR, Ginsburg KS, Bers DM. SR Ca uptake rate in permeabilized ventricular myocytes is limited by reverse rate of the SR Ca pump. *Biophys J*. 1997;72:A167.

40. Vermeulen JT, McGuire MA, Opthof T, Colonel R, de Bakker JMT, Klopping C, Janse MJ. Triggered activity and automaticity in ventricular trabeculae of failing human and rabbit hearts. *Cardiovasc Res*. 1994;28: 1547–1554.

41. Li HG, Jones DL, Yee R, Klein GJ. Electrophysiologic substrate associated with pacing-induced heart failure in dogs: potential value of programmed stimulation in predicting sudden death. *J Am Coll Cardiol*. 1992;19:444–449.

42. Beuckelmann DJ, Nabauer M, Erdmann E. Intracellular calcium handling in isolated ventricular myocytes from patients with terminal heart failure. *Circulation*. 1992;85:1046–1055.

43. Gwathmey JK, Copelas L, MacKinnon R, Schoen FJ, Feldman MD, Grossman W, Morgan JP. Abnormal intracellular calcium handling in myocardium from patients with end-stage heart failure. *Circ Res*. 1987; 61:70–76.

44. Stern MD. Theory of excitation-contraction coupling in cardiac muscle. *Biophys J*. 1992;63:497–517.

45. Gomez AM, Valdivia HH, Cheng H, Lederer MR, Santana LF, Cannell MB, McCune SA, Altschuld RA, Lederer WJ. Defective excitation-contraction coupling in experimental heart cardiac hypertrophy and heart failure. *Science*. 1997;276:800–806.

46. Langer GA, Peskoff A. Calcium concentration and movement in the diadic cleft space of the cardiac ventricular cell. *Biophys J*. 1996;70: 1169–1182.

47. Cannell MB, Soeller C. Numerical analysis of ryanodine receptor activation by L-type channel activity in the cardiac muscle diad. *Biophys J*. 1997;73:112–122.

48. Soeller C, Cannell MB. Numerical simulation of local calcium movements during L-type calcium channel gating in the cardiac diad. *Biophys J*. 1997;73:97–111.

49. Wagner J, Keizer J. Effects of rapid buffers on Ca2+ diffusion and Ca2+ oscillations. *Biophys J*. 1994;67.

50. Fiset C, Clark RB, Shimoni Y, Giles WR. Shal-type channels contribute to the Ca^{2+}-independent transient outward K^+ current in rat ventricle. *J Physiol (Lond)*. 1997;500:51–64.

51. Johns DC, Nuss HB, Marban E. Suppression of neuronal and cardiac transient outward current by viral gene transfer of dominant negative Kv4.2 constructs. *J Biol Chem*. 1997;272:31598–31603.

52. Kubiček M, Marek M. *Computational Methods in Bifurcation Theory and Dissipative Structures*. New York, NY: Springer-Verlag; 1983.